PLOS | COMPUTATIONAL BIOLOGY

Resolving Anatomical and Functional Structure in Human Brain Organization: Identifying Mesoscale Organization in Weighted Network Representations

Christian Lohse[1], Danielle S. Bassett[2,3,4]*, Kelvin O. Lim[5], Jean M. Carlson[2]

1 Kirchhoff Institute for Physics, University of Heidelberg, Heidelberg, Germany, 2 Department of Physics, University of California, Santa Barbara, California, United States of America, 3 Sage Center for the Study of the Mind, University of California, Santa Barbara, California, United States of America, 4 Department of Bioengineering, University of Pennsylvania, Philadelphia, Pennsylvania, United States of America, 5 Department of Psychiatry, University of Minnesota, Minneapolis, Minnesota, United States of America

Abstract

Human brain anatomy and function display a combination of modular and hierarchical organization, suggesting the importance of both cohesive structures and variable resolutions in the facilitation of healthy cognitive processes. However, tools to simultaneously probe these features of brain architecture require further development. We propose and apply a set of methods to extract cohesive structures in network representations of brain connectivity using multi-resolution techniques. We employ a combination of soft thresholding, windowed thresholding, and resolution in community detection, that enable us to identify and isolate structures associated with different weights. One such *mesoscale* structure is bipartivity, which quantifies the extent to which the brain is divided into two partitions with high connectivity between partitions and low connectivity within partitions. A second, complementary mesoscale structure is modularity, which quantifies the extent to which the brain is divided into multiple communities with strong connectivity within each community and weak connectivity between communities. Our methods lead to multi-resolution curves of these network diagnostics over a range of spatial, geometric, and structural scales. For statistical comparison, we contrast our results with those obtained for several benchmark null models. Our work demonstrates that multi-resolution diagnostic curves capture complex organizational profiles in weighted graphs. We apply these methods to the identification of resolution-specific characteristics of healthy weighted graph architecture and altered connectivity profiles in psychiatric disease.

Introduction

Noninvasive neuroimaging techniques provide quantitative measurements of structural and functional connectivity in the human brain. Functional magnetic resonance imaging (fMRI) indirectly resolves time dependent neural activity by measuring the blood-oxygen-level-dependent (BOLD) signal while the subject is at rest or performing a cognitive task. Diffusion weighted imaging (DWI) techniques use MRI to map the diffusion of water molecules along white matter tracts in the brain, from which anatomical connections between brain regions can be inferred. In each case, measurements can be represented as a weighted network [1,2,3,4,5,6,7], in which nodes correspond to brain regions, and the weighted connection strength between two nodes can, for example, represent correlated activity (fMRI) or fiber density (DWI). The resulting network is complex, and richly structured, with weights that exhibit a broad range of values, reflecting a continuous spectrum from weak to strong connections.

The network representation of human brain connectivity facilitates quantitative and statistically stringent investigations of human cognitive function, aging and development, and injury or disease. Target applications of these measurements include disease diagnosis, monitoring of disease progression, and prediction of treatment outcomes [8,9,10,11,12]. However, efforts to develop robust methods to reduce these large and complex neuroimaging data sets to statistical diagnostics that differentiate between patient populations have been stymied by the dearth of methods to quantify the statistical significance of apparent group differences in network organization [13,14,15,16].

Network comparisons can be performed in several ways. In one approach, network comparisons are made after applying a threshold to weighted structural and functional connectivity matrices to fix the number of edges at a constant value in all individuals [4,13]. Edges with weights passing the threshold are set to a value of 1 while all others are set to a value of 0 (a process referred to as 'binarizing'). In some cases results are tested for robustness across multiple thresholds, although this increases the probability of Type I (false positive) errors from multiple non-independent comparisons. More generally, this procedure disregards potentially important neurobiological information present in

Author Summary

The human brain is a fascinating organ full of exquisite anatomical and functional detail. A striking feature of this detail lies in the presence of small modules nested within one another across hierarchical levels of organization. Here we develop and apply computational analysis tools to probe these features of brain architecture by examining network representations in which brain areas are treated as network nodes and links between areas are treated as network edges. The class of methods that we describe are referred to as "multi-resolution techniques" and enable us to identify and isolate neural structures associated with different edge properties. Our methods lead to multi-resolution curves of these network diagnostics over a range of spatial, geometric, and structural scales. For statistical comparison, we contrast our results with those obtained for several benchmark null models. Our work demonstrates that multi-resolution diagnostic curves capture complex organizational profiles in weighted graphs. We apply these methods to the identification of resolution-specific characteristics of healthy weighted graph architecture and altered connectivity profiles in psychiatric disease.

the original edge weights. A second approach involves examination of network geometry in the original weighted matrices without binarizing. However, because the values of weighted metrics can be influenced by both the average weight of the matrix and the distribution of weights, this approach presents peculiar complications for the assessment of group differences [14,15]. Critically, neither of these two approaches for network comparison allow for a principled examination of network structure as a function of weight (strong versus weak connections) or space (short versus long connections). Disease-related group differences in network architecture that are present only at a particular edge weight range or at a specific spatial resolution can therefore remain hidden.

In this paper, we employ several techniques to examine the multi-resolution structure of weighted connectivity matrices: soft thresholding, windowed thresholding, and modularity resolution. A summary of these techniques is presented in Table 1, and each method is discussed in more detail in the Methods section. We apply these techniques to two previously published data sets: structural networks extracted from diffusion tractography data in five healthy human subjects [17] and functional networks extracted from resting state fMRI data in people with schizophrenia and healthy controls (N = 58) [15]. As benchmark comparisons, we also explore a set of synthetic networks that includes a random Erdős-Rényi network (ER), a ring lattice (RL), a small-world network (SW), and a fractal hierarchical network (FH).

While multi-resolution techniques could be usefully applied to a broad range of network diagnostics, here we focus on two complementary mesoscale characteristics that can be used to probe the manner in which *groups* of brain regions are connected with one another: modularity and bipartivity. Modularity quantifies community structure in a network by identifying groups of brain regions that are more strongly connected to other regions in their group than to regions in other groups [18,19]. Communities of different sizes, nested within one another, have been identified in both structural and functional brain networks [20,21,22,23,24] and are thought to constrain information processing [25,26,27]. Bipartivity quantifies bipartite structure in a network by separating brain regions into two groups with sparse connectivity within each group and dense connectivity between the two groups. The dichotomous nature of bipartivity is particularly interesting to quantify in systems with bilateral symmetry such as the human brain, in which inter- and intra-hemispheric connectivity display differential structural [28] and functional [29] network properties.

We describe these techniques, diagnostics, and null models in detail in the Methods section and illustrate their utility in addressing questions in systems and clinical neuroscience in the Results section.

Methods

This section has three major components: (1) a description of the empirical data examined in this study as well as the simpler synthetic networks employed to illustrate our techniques in well-characterized, controlled settings, (2) a summary of the graph diagnostics used in our analysis to examine properties of mesoscale network architecture, and (3) definitions of the soft thresholding, windowed thresholding, and modularity resolution techniques which provide a means to resolve network structure at different connection strengths.

Empirical and Synthetic Benchmark Networks

We examine two separate neuroimaging data sets acquired noninvasively from humans. The first is a set of $N = 6$ structural networks constructed from diffusion spectrum imaging (DSI) data (taken from 5 subjects; one subject was scanned twice) and the second is a set of $N = 58$ functional networks constructed from resting state functional magnetic resonance imaging (fMRI) data. For comparison, we generate 4 types of synthetic network models that range from an Erdős-Rényi random graph to models that include more complex structure, including hierarchy and clustering.

Each network is described by an adjacency matrix $\mathbf{A}$ whose ij^{th} entry describes the weight of the edge connecting nodes i and j. For the empirical brain networks, the edge weights are determined by neuroimaging measurements. For the synthetic networks, we construct weights to mimic the structural organization of the network, as described below.

Empirical brain networks: Data acquisition and preprocessing. Because our focus in this paper lies in method development and illustration, we have chosen to utilize two previously published empirical brain network data sets. These data sets were chosen to represent the two neuroimaging techniques most commonly utilized for analysis of brain network architecture: diffusion imaging which captures anatomical structure, and fMRI which captures brain function. For our diffusion data set, we chose the DSI data from the seminal contribution of Hagmann et al. 2008 in PLoS Biol [17]. For our fMRI data set, we chose a resting state data set acquired from both healthy controls and a patient population to enable the comparison of multiresolution structure in two sets of networks, thereby illustrating the utility of these techniques in the context of clinical questions [15]. In both data sets, we utilized the brain networks extracted and examined in these two papers [17,15], enabling a direct comparison between the utility of multiresolution techniques and previously published single resolution techniques.

Structural networks:. We construct an adjacency matrix $\mathbf{A}$ whose ij^{th} entries are the probabilities of fiber tracts linking region i with region j as determined by an altered path integration method. The resultant adjacency matrix $\mathbf{A}$ contains entries A_{ij} that represent connection weights between the 998 regions of interest extracted from the whole brain. We also define the distance matrix $\mathbf{L}$ to contain entries L_{ij} that are the average curvilinear distance traveled by fiber tracts that link region i with region j, or the Euclidean distance between region i and j, where

Table 1. Summary of multi-resolution methods for network diagnostics.

Technique	Method Summary	Control Parameter	Strengths and Limitations	Refs.
Soft Threhsolding	Raise each entry in $\mathbf{A}$ to the power r:$A_{ij} \rightarrow A_{ij}^r$	r: power applied to entries in $\mathbf{A}$. Small r limit weights all connections equally. Large r limit amplifies strong connections, relative to weak.	Enables continuous variation of the contribution of edges of different weights. Strong edges may dominate, but all connections retained.	[49,50]
Windowed Thresholding	Construct binarized network a fixed percentage of connections corresponding to a range of edge weights	g: average edge weight of connections within the window. Small g isolates weak connections. Large g isolates strong connections.	Enables an isolated view of structure at different edge weights. Weak connections are not obscured by strong connections, but relationships between strong and weak connections are ignored.	[15,49]
Modularity Resolution	Structural resolution tuned in community detection. Sets a tolerance on the partition into modules relative to a null model.	γ: appears in the quality function Q_b or Q_w optimized when dividing nodes into partitions. Small γ yields one large community. Large γ yields many small communities.	Enables a continuous variation in the resolution of community structure. This method has the most direct, tunable control of the output, but does not generalize to diagnostics other than those associated with modularity.	[51]

We use soft thresholding, windowed thresholding, and variation in the resolution parameter of modularity maximization to probe network architecture across scales (Column 1). For each approach, we provide a method summary (Column 2), a description of the control parameter (Column 3), a brief synopsis of the strengths and limitations of the approach (Column 4), and a few relevant references (Column 5).

no data of the arc length was available. We define separate $\mathbf{A}$ and $\mathbf{L}$ adjacency matrices for each of 5 healthy adults with 1 adult scanned twice (treated as 6 separate scans throughout the paper). For further details, see [17].

Functional networks: We construct an adjacency matrix $\mathbf{A}$ whose ij^th entry is given by the absolute value of the Pearson correlation coefficient between the resting state wavelet scale 2 (0.06–0.12 Hz) blood oxygen level dependent (BOLD) time series from region i and from region j. The resultant adjacency matrix $\mathbf{A}$ contains entries A_{ij} that represent functional connection weights between 90 cortical and subcortical regions of interest extracted from the whole brain automated anatomical labeling (AAL) atlas [30].

We define separate adjacency matrices for each of 29 participants with chronic schizophrenia (11 females; age 41.3 ± 9.3 (SD)) and 29 healthy participants (11 females; age 41.1 ± 10.6 (SD)) (see [31] for detailed characteristics of participants and imaging data). We note that the two groups had similar mean RMS motion parameters (two-sample t-tests of mean RMS translational and angular movement were not significant at $p = 0.14$ and $p = 0.12$, respectively), suggesting that identified group difference in network properties could not be attributed to differences in movement during scanning.

Synthetic benchmark networks. In addition to empirical networks, we also examine 4 synthetic model networks to illustrate our techniques in well-characterized, controlled settings: an Erdös-Rényi random network, a ring-lattice, a small world network, and a fractal hierarchical network (see Fig. 9). These four network models provide simple benchmark comparisons for the empirical data but cannot be interpreted as biological models of the empirical data. Indeed, the question of which graphical models produce networks most similar to empirical data is a matter of ongoing investigation [28]. All networks were created using modified code from [32].

The Erdös-Rényi and the ring-lattice networks are important benchmark models used in a range of contexts across a variety of network systems. Small world and fractal hierarchical networks incorporate clustering and layered structure, reminiscent of

properties associated with brain networks [33]. We emphasize that the synthetic models are not intended to be realistic models of the brain. Rather, we use them to isolate structural drivers of network topology and to illustrate the utility of multi-resolution approaches [34] in a controlled setting.

Most synthetic network models, including all those that we study in this paper were originally developed as binary graphs (i.e. all edge weights equal to either 0 or 1). Since we are specifically interested in the effect of edge weights on network properties, we consider weighted generalizations of these models, in which the weights of edges are chosen to maintain essential structural properties of the underlying graph (see Figure 9). For example, in network models that display hierarchical structure, edge weights differ across the hierarchical levels but remain constant within a hierarchical level, while in network models with both short and long distance topological connections, edge weights correspond to the topological distance of connections (see below for additional details). Importantly, all of these networks therefore maintain the same number of nodes and edges as the empirical data, but differ in terms of their average weight, degree distribution, and strength distribution as expected mathematically from the differences in their geometry (i.e., weighted network structure).

Erdös-Rényi Random (ER) model: The Erdös-Rényi random graph serves as an important benchmark null model against which to compare other empirical and synthetic networks. The graph $G(N,K)$ is constructed by assigning a fixed number of connections K between the N nodes of the network. The edges are chosen uniformly at random from all possible edges, and we assign them weights drawn from a uniform distribution in $[0,1]$.

Ring-Lattice (RL) model: The one-dimensional ring-lattice model can be constructed for a given number of edges K and number of nodes N by first placing edges between nodes separated by a single edge, then between pairs of nodes separated by 2 edges and so on, until all K connections have been assigned. To construct a geometric (i.e. weighted) chain-like structure, we assign the weights of each edge to mimic the topological structure of the binary chain lattice. Edge weights decreased linearly from 1 to 0 with increasing topological distance between node pairs.

Small World (SW) model: Networks with high clustering and short path lengths are often referred to as displaying "small world" characteristics [35,36]. Here we construct a modular small world model [33] by connecting $N = 2^n$ nodes in elementary groups of fully connected clusters of $M = 2^m$ nodes, where m and n are integers. If the number of edges in this model is less than K, the remaining edges are placed uniformly at random throughout the network. The edges in this model are either intra-modular (placed within elementary groups) or inter-modular (placed between elementary groups). To construct a geometrical modular small world model, we assigned different weights to the two types of edges: $A_{ij} = 1$ for intra-modular edges and $A_{ij} = 0.5$ for inter-modular edges.

To ensure our comparisons are not dominated by the overall network density, we construct synthetic network models with N nodes and K edges to match the empirical data [13]. For modular small world networks, this stipulation requires that we modify the algorithm above to produce networks in which the number of nodes is not necessarily an exact power of two. For comparisons to the structural (functional) brain data, we generate a model as described above with $N = 1024, M = 8$ ($N = 128, M = 4$) and then chose 24 (38) nodes at random, which are deleted along with their corresponding edges.

Fractal Hierarchical (FH) model: Network structure in the brain displays a hierarchically modular organization [20,21,22,23,24] thought generally to constrain information processing phenomena [26,27,28]. Following [33,37], we create a simplistic model consisting of $N = 2^n$ nodes that form $l_{max} \leq n$ hierarchical levels to capture some essential features of fractal hierarchical geometry in an idealized setting. At the lowest level of the hierarchy, we form fully connected elementary groups of size $M = 2^m, m = n - l_{max} + 1$ and weight all edges with the value 1. At each additional level of the hierarchy l, we place edges uniformly at random between two modules from the previous level $l - 1$. The density of these inter-modular edges is given by the probability $p(l) = E^{-l}$ where E is a control parameter chosen to match the connection density $\frac{K}{N(N-1)}$ of the empirical data set. To mimic this defining topological feature, we construct the network geometry by letting edge weights at level l equal $p(l)$. For comparisons to the structural (functional) brain data, we generate a model as described above with $N = 1024, M = 8$ $l_{max} = 7$ ($N = 128, M = 4, l_{max} = 7$) and then chose 24 (38) nodes at random, which are deleted along with their corresponding edges.

Constructing network ensembles. Each empirical data set displays variable K values. To construct comparable ensembles of synthetic networks, we drew K from a Gaussian distribution defined by the mean and standard deviation of K in the empirical data. For comparisons to DSI empirical data, we constructed ensembles of $N = 1000, K = (2.88 \pm 0.10) \cdot 10^4$ composed of 50 realizations per model. See Supplementary Information Table S1 for details on the ensembles.

Mesoscale Network Diagnostics

In this paper we focus on two, complementary network characteristics that can be used to probe the manner in which *groups* of brain regions are connected with one another: modularity and bipartivity. These methods, however, are more generally applicable, and could be used to evaluate weight dependence of other metrics and data sets as well [38].

Community detection and modularity. Community detection by modularity maximization identifies a partition of the nodes of a network into groups (or *communities*) such that nodes are more densely connected with other nodes in their group than

expected in an appropriate statistical null model. In this paper, we use this method to extract values of network modularity and other related diagnostics including community laterality, community radius, and the total number and sizes of communities. An additional feature of modularity maximization that is particularly useful for our purposes is its resolution dependency, which enables us to continuously monitor diagnostic values over different organizational levels in the data.

Community detection can be applied to both binary and weighted networks. Assuming node i is assigned to community c_i and node j is assigned to community c_j, the quality of a partition for a binary network is defined using a modularity index [18,19,39,40,41]:

$$Q_b = \frac{1}{2K} \sum_{i,j} (B_{ij} - \gamma P_{ij}) \delta(c_i, c_j), \qquad (1)$$

where $\frac{1}{2K}$ is a normalization constant, **B** is the binary adjacency matrix, γ is a structural resolution parameter, and P_{ij} is the probability of a connection between nodes i and j under a given null model. Here we use the Newman-Girvan null model [40] that defines the connection probability between any two nodes under the assumption of randomly distributed edges and the constraint of a fixed degree distribution: $P_{ij} = \frac{k_i k_j}{2K}$, where k_i is the degree of node i. We optimize Q_b from Equation 1 using a Louvain-like [42] locally greedy algorithm [43] to identify the optimal partition of the network into communities.

For weighted networks, a generalization of the modularity index is defined as [44,45]:

$$Q_w = \frac{1}{2W} \sum_{i,j} (A_{ij} - \gamma \frac{s_i s_j}{2W}) \delta(c_i, c_j), \qquad (2)$$

where $W = \frac{1}{2} \sum_{ij} A_{ij}$ is the total edge weight, **A** is the weighted adjacency matrix, and s_i is the strength of node i defined as the sum of the weights of all edges emanating from node i.

Due to the non-unique, but nearly-degenerate algorithmic solutions for Q_b and Q_w obtained computationally [46], we perform 20 optimizations of Equation 1 or 2 for each network under study. In the results, we report mean values of the following 4 diagnostics over these optimizations: the modularity Q_b or Q_w, the number of communities, the number of singletons (communities that consist of only a single node), and the community laterality and radius (defined in a later sections). We observed that the optimization error in these networks is significantly smaller than the empirical inter-individual or synthetic inter-realization variability, suggesting that these diagnostics produce reliable measurements of network structure (see Supplementary Information).

Community laterality. Laterality is a property that can be applied to any network in which each node can be assigned to one of two categories, and within the community detection method, describes the extent to which a community localizes to one category or the other [29]. In neuroscience, an intuitive category is that of the left and right hemispheres, and in this case laterality quantifies the extent to which the identified communities in functional or structural brain networks are localized within a hemisphere or form bridges between hemispheres.

For an individual community c within the network, the laterality Λ_c is defined as [29]:

$$\Lambda_c = \frac{|N_r - N_l|}{N_c}, \tag{3}$$

where N_r and N_l are the number of nodes located in the left and right hemispheres respectively, or more generally in one or other of the two categories, and N_c is the total number of nodes in c. The value of l ranges between zero (i.e., the number of nodes in the community are evenly distributed between the two categories) and unity (i.e., all nodes in the community are located in a single category).

We define the laterality of a given partition of a network as:

$$\Lambda = \frac{1}{N}\left(\sum_c N_c \Lambda_c - \left\langle \sum_c N_c \Lambda_c \right\rangle\right), \tag{4}$$

where we use $\langle \sum_c N_c \Lambda_c \rangle$ to denote the expectation value of the laterality under the null model specified by randomly reassigning nodes to the two categories while keeping the total number of nodes in each category fixed. We estimate the expectation value by calculating $\sum_c N_c \Lambda_c$ for 1000 randomizations of the data, which ensures that the error in the estimation of the expectation value is of order 10^{-3}.

The laterality of each community is weighted by the number of nodes it contains, and the expectation value is subtracted to minimize the dependence of Λ on the number and sizes of detected communities. This correction is important for networks like the brain that exhibit highly fragmented structure. Otherwise the estimation would be biased by the large number of singletons, that by definition have a laterality of $\Lambda_c = 1.0$.

Community radius: To measure the spatial extent of a community in a physically embedded network such as the human brain, we suggest the notion of a community 'radius'. Each node in the brain network has a position in physical space, which can be delineated by x, y, and z coordinates and which we refer to as that node's position vector. We calculate the standard deviation s_i of the position vectors x along each dimension i. Then we estimate the radius of the community as the length of the standard deviation vector s as follows:

$$\rho_c = \frac{1}{N_c}\left(N \sum_{i \in c} \|\mathbf{r}_i\|^2 - \|\sum_{i \in c} \mathbf{r}_i\|^2\right)^{\frac{1}{2}}, \tag{5}$$

where N_c is the number of nodes in community c and $\mathbf{r}_i$ is the position vector of node i.

The average community radius of the entire network $\mathbf{A}$ is

$$\rho_A = \frac{1}{N}\sum_c N_c \frac{\rho_c}{R_A}, \tag{6}$$

where N_c serves to weight every community by the number of nodes it contains (compare to Equation 4), and R_A is a normalization constant equal to the 'radius' of the entire network: $R_A = \frac{1}{N}\sqrt{\left(\sum_{i=1}^N \|\mathbf{r}_i\|^2 - \|\sum_{i=1}^N \mathbf{r}_i\|^2\right)}$. In this investigation, community radius is evaluated only for the empirical brain networks, since the synthetic networks lack a physical embedding.

Bipartivity. Bipartivity is a topological network characteristic that occurs naturally in certain complex networks with two types of nodes. A network is perfectly bipartite if it is possible to separate the nodes of the network into two groups, such that all edges lie between the two groups and no edges lie within a group. In this

sense bipartivity is a complementary diagnostic to modularity, which maximizes the number of edges within a group and minimizes the number of edges between groups.

Most networks are not perfectly bipartite, but still show a certain degree of bipartivity. A quantitative measure of bipartivity can be defined by considering the subgraph centrality $\langle SC \rangle$ of the network, which is defined as a weighted sum over the number of closed walks of a given length. Because a network is bipartite if and only if there only exist closed walks of even length, the ratio of the contribution of closed walks of even length to the contribution of closed walks of any length provides a measure of the network bipartivity [47]. As shown in [47], this ratio can be calculated from the eigenvalues λ_j of the adjacency matrix [47]:

$$\beta = \frac{\langle SC_{even} \rangle}{\langle SC \rangle} = \frac{\sum_{\lambda_j} \cosh(\lambda_j)}{\sum_{\lambda_j} \exp(\lambda_j)}, \tag{7}$$

where $\langle SC_{even} \rangle$ is the contribution of closed walks of even length to the subgraph centrality. In this formulation, β takes values between 0.5 for the least bipartite graphs (fully connected graphs) and 1.0 for a perfectly bipartite graph [47].

The definition of bipartivity given in Equation 7 provides an estimate of β but does not provide a partition of network nodes into the two groups. To identify these partitions, we calculate the eigenvector corresponding to the smallest eigenvalue λ_{min} of the modularity quality matrix $M_{ij} = \frac{1}{2K}(A_{ij} - \frac{k_i k_j}{2K})$ [48]. We then partition the network according to the signs of the entries of this eigenvector: nodes with positive entries in the eigenvector form group one and nodes with negative entries in the eigenvector form group two. This spectral formulation demonstrates that bipartivity is in some sense an anti-community structure [48]: community structure corresponds to the highest eigenvalues of $\mathbf{M}$ while the bipartivity corresponds to the lowest eigenvalue of $\mathbf{M}$.

Multi-Resolution Methods

We quantify organization of weighted networks across varying ranges of connection weights (weak to strong) and connection lengths (short to long), using three complementary approaches: soft thresholding, windowed thresholding, and multi-resolution community detection. Each method employs a control parameter that we vary to generate network diagnostic curves, representing characteristics of the network under study. We refer to these curves as *mesoscopic response functions* (MRF) of the network [34]. A summary of the methods and control parameters is contained in Table 1.

Soft thresholding. To date, most investigations that have utilized thresholding to study brain networks have focused on *cumulative* thresholding [4], where a weighted network is converted to a binary network (binarized) by selecting a single threshold parameter τ and setting all connections with weight $A_{ij} > \tau$ to 1 and all other entries to 0. Varying τ produces multiple binary matrices over a wide range of connection densities (sparsity range). On each of these matrices, we can compute a network diagnostic of interest. One disadvantage of this *hard* thresholding technique is that it assumes that matrix elements with weights just below τ are significantly different from weights just above τ.

Soft thresholding [49,50] instead probes the full network geometry as a function of edge weight. First, we normalize edge weights to ensure that all A_{ij} are in [0,1]. Next, we create a family of graphs from each network by reshaping its weight distribution by taking the adjacency matrix to the power r: $A_{ij} \to A_{ij}^r$. At each value of r, the distribution of edge weights – and by extension, the

network geometry – is altered. As r goes towards zero, all nonzero elements of the matrix have larger and larger weights. At $r=0$, the weight distribution approximates a delta function: all nonzero elements of the resulting matrix have the same weight of $A_{ij}^r=1$, which corresponds to the application of a hard threshold at $\tau=0$. At $r\to\infty$, the weight distribution is heavy-tailed: the majority of elements of the resulting matrix are equal to 0, corresponding to the application of a hard threshold at $\tau\to\max_{ij}A_{ij}$.

Windowed thresholding. A potential disadvantage of both the cumulative and soft thresholding approaches is that results may be driven by effects of both connection density and the organization of the edges with the largest weights. As a result, these procedures can neglect underlying structure associated with weaker connections.

Windowed thresholding [15,49] instead independently probes the topology of families of edges of different weights. We replace the cumulative threshold τ with a threshold window $[g_-,g_+]$ that enforces an upper and lower bound on the edge weights retained in the construction of a binary matrix. We can specify this window using two parameters: (i) a fixed percentage p of connections which are retained in each window, and (ii) the average percentile weight g of connections in each window. Note that we refer to the average percentile edge weight g in the remainder of this document as the *connection weight*. For example, if we specify $p=0.10$ and $g=0.40$, then we can identify the values g, g_- and g_+ (here given as percentiles of all connections) that provide a set of $p*K$ edges whose average percentile edge weight is 0.40. Each pair of variables (p,g) ensures a unique set of edges.

More specifically, for each network $\mathbf{A}$, we construct a family of binary graphs $\mathbf{B}^p(g)$, each of which depends on the window size p (percentage of connections retained), and the average weight g of connections in the window (together p and g determine the upper and lower bounds, g_- and g_+, defining the window):

$$B_{ij}^p(g) = \begin{cases} 1, & \text{if } A_{ij} \in [g_-, g_+]; \\ 0, & \text{otherwise.} \end{cases} \qquad (8)$$

The fixed window size (5%–25%) mitigate biases associated with variable connection densities [4,14,15]. Each resulting binary graph $\mathbf{B}^p(g)$ in the family summarizes the topology of edges with a given range of weights. The window size sets a resolution limit to the scale on which one can observe weight dependent changes in structure (see the Supplementary Information).

To probe the roles of weak versus strong edges and short versus long edges in the empirical brain networks, we extract families of graphs based on (i) networks weighted by correlation strength (fMRI), (ii) networks weighted by number of white matter streamlines (DSI), (iii) networks weighted by Euclidean distance between brain regions (DSI), and (iv) one network weighted by fiber tract arc length (DSI). For each case we compute graph diagnostics as a function of the associated connection weight g. This method isolates effects associated with different connection weights, but does not resolve network organization across different ranges of weights.

Resolution in community detection. The definition of modularity in Equations 1,2 includes a resolution parameter γ [51,52,53] which tunes the size of communities in the optimal partition: high values of γ lead to many small communities and low values of γ lead to a few large communities. We vary γ to explore partitions with a range of mean community sizes: for the smallest value of γ the partition contains a single community of size N, while for the largest value of γ the partition contains N

communities of size unity. In physically embedded systems, such as brain networks, one can probe the relationship between structural scales uncovered by different γ values and spatial scales defined by the mean community radius ρ.

Results

Multi-resolution methods serve as tools to investigate the structure of networks in ways that are unapproachable to single-resolution methods. What types of multi-resolution structure might be present in a network? One type of multi-resolution structure corresponds to the properties of individuals edges. In weighted embedded networks, for example, edges have both weights and lengths, and therefore network architecture might vary over both weight- or length-scales, and even perhaps differently over these two scales. Understanding this multi-resolution structure can inform our interpretations of network diagnostics and can provide mathematical means to distinguish between real and synthetic networks or between healthy and diseased brain networks.

To illustrate these points, we apply multi-resolution diagnostics to a sequence of 5 problems involving weighted empirical and synthetic network data (see Fig. 1). Problem 1 illustrates the utility of multi-resolution methods in informing our interpretations of network diagnostics. Problems 2 and 5 illustrate the utility of multi-resolution methods in distinguishing different types of networks. Problems 3 and 4 illustrate how multi-resolution structure in networks can differ across weight and length scales. We summarize each of these problems in more detail below.

- **Problem 1: Probing Drivers of Weighted Modularity.** We begin our analysis with the weighted modularity Q_w (Equation 2), a diagnostic that is based on the full weighted adjacency matrix. Using soft thresholding, we show that Q_w is most sensitive to the strongest connections. This motivates the use of windowed thresholding to isolate the topology of connections based on their weight.

- **Problem 2: Determining Network Differences in Multiresolution Structure.** In anatomical brain data and corresponding synthetic networks, we use windowed thresholding to obtain multi-resolution response functions (MRFs) for modularity $Q_b(g)$ and bipartivity $\beta(g)$ as a function of the average weight g within the window. MRFs of synthetic networks do not resemble MRFs of the brain.

- **Problem 3: Uncovering Differential Structure in Edge Strength & Length.** Using windowed thresholding, we probed the multiresolution structure in anatomical brain data captured by two measures of connection weight: fiber density and fiber length. We observe that communities involving short, high density fibers tend to be localized in one hemisphere, while communities involving long, low density fibers span the hemispheres.

- **Problem 4: Identifying Physical Correlates of Multi-resolution Structure.** To investigate structure that spans geometric scales, we vary the resolution parameter in modularity maximization to probe mesoscale structure at large (few communities) and small scales (many communities). By calculating community radius, we find that large communities, as measured by the number of nodes, are embedded in large physical spaces.

- **Problem 5: Demonstrating Clinical Relevance.** To test diagnostic applicability, we apply our methods to functional (fMRI) networks extracted from a people with schizophrenia and healthy controls. Using windowed thresholding, we observe previously hidden significant differences between the
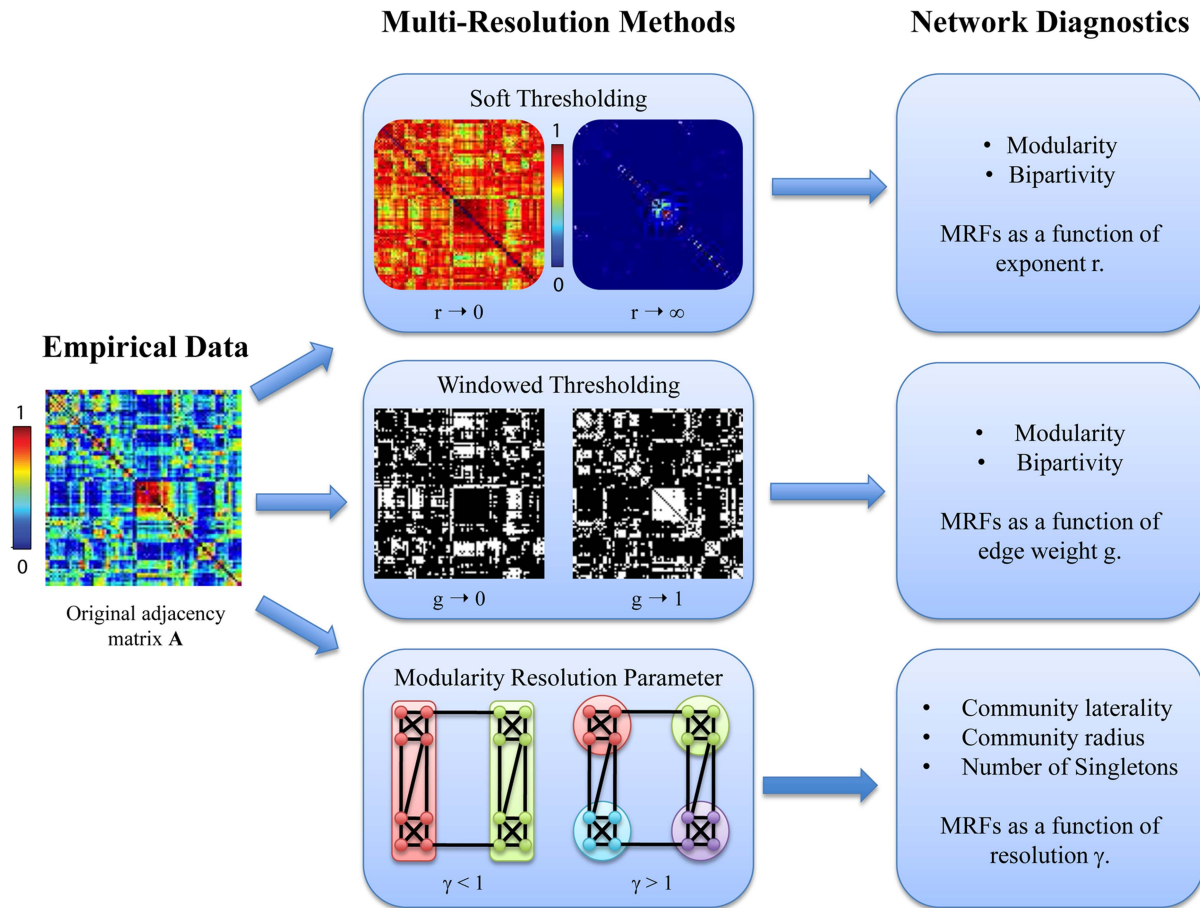
Multi-Resolution Methods

Network Diagnostics

Figure 1. Pictorial schematic of multi-resolution methods for weighted networks. We can apply soft or windowed thresholding, and vary the resolution parameter of modularity maximization to uncover multiresolution structure in empirical data that we summarize in the form of MRFs of network diagnostics.
doi:10.1371/journal.pcbi.1003712.g001

two groups in specific weight ranges, suggesting that multi-resolution methods provide a powerful approach to differentiating clinical groups.

In the remainder of this Results section, we describe each of these problems and subsequent observations in greater detail.

Probing Drivers of Weighted Modularity

In this first section, we examine Problem 1: Probing Drivers of Weighted Modularity. We begin our analysis with measurements that illustrate the sensitivity of mesoscale network diagnostics to the edge weight organization and distribution. We employ the weighted modularity Q_w to characterize the community structure of the network and ask whether the value of this diagnostic is primarily driven by the organization of strong edges or by the organization of weak edges. To answer this question, we will utilize two methods: network rewiring and soft thresholding.

Rewiring. By randomly rewiring connections in a weighted network, one can quantify which connections dominate the value of the diagnostic in the original adjacency matrix. In empirical DSI data and three synthetic networks, we compare results obtained when a percentage p of the connections are rewired, starting with the strongest connections (solid lines) or starting with the weakest connections (dashed lines); see Fig. 2. We observe that modularity Q_w as a function of rewiring percentage p depends on

the network topology. Randomly rewiring an Erdös-Rényi network has no effect on Q_w since it does not alter the underlying geometry. However, randomly rewiring a human DSI network or a synthetic fractal hierarchical or ring lattice network leads to changes in Q_w, that moreover depend on the types of edges rewired. Rewiring a large fraction of the weakest edges has a negligible effect on the value of Q_w, while rewiring even a few of the strongest edges decreases the value of Q_w drastically in all three networks. These results illustrate that the value of Q_w is dominated by a few edges with the largest weights. For additional contributions to Q_w from the number of singletons in the network, see Supplementary Figure S4 and accompanying text.

Soft thresholding. To more directly examine the role of edge weight in the value of the maximum modularity, we employ soft thresholding, which individually raises all entries in the adjacency matrix to a power r (see the Methods Section for methodological details and Fig. 1 for a schematic). Small values of r tend to equalize the original weights, while larger values of r increasingly emphasize the stronger connections. By varying r, we can probe similarities and differences in both the weight distributions and weight geometries. In Fig. 3 we evaluate the mesoscopic response function (MRF) Q_w as a function of r, for empirical functional (fMRI) brain networks, as well as two synthetic networks. While the range of r most useful to study in any particular scientific investigation is an open question, here we
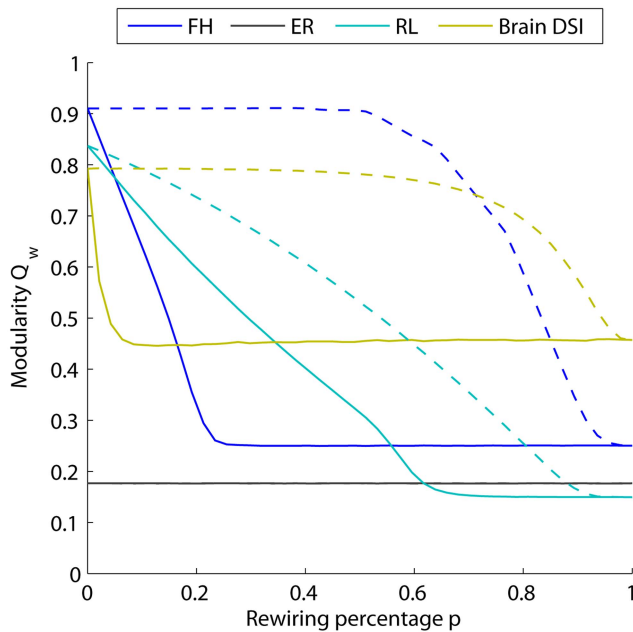
Figure 2. Use of rewiring strategies to probe geometric drivers of weighted modularity. Changes in the maximum modularity as a given percentage p of the connections are randomly rewired for synthetic (fractal hierarchical, *FR*, in blue; Erdös-Rényi, *ER*, in black; ring lattice, *RL*, in cyan) and empirical (Brain DSI in mustard) networks. Dashed lines show the change of modularity when the p weakest connections are randomly rewired; solid lines illustrate the corresponding results when the p strongest connections are rewired. For the brain data and the synthetic networks, the value of the weighted modularity Q_w is most sensitive to the strongest connections in both the synthetic and empirical networks.
doi:10.1371/journal.pcbi.1003712.g002

Figure 3. Use of soft thresholding strategies to probe geometric drivers of weighted modularity. Changes in maximum modularity $Q_w(r)$ as a function of the control parameter r for soft thresholding. MRFs are presented for synthetic (fractal hierarchical, *FR*, in blue; Erdös-Rényi, *ER*, in black) and empirical (Brain fMRI in red) networks. Dots mark the peak value for different curves, which occur at different values of r. The vertical dashed line marks the conventional value of Q_w obtained for $r=1$. The single, point summary statistic $Q_w(r=1)$ fails to capture the full structure of the MRF revealed using soft thresholding.
doi:10.1371/journal.pcbi.1003712.g003

vary r from 10^{-4} to 10^4. Our results illustrate that $Q_w(r)$ varies both in shape and limiting behavior for different networks.

In the limit of $r \to 0$, the sparse networks (FH and ER) all converge to a non-zero value of Q_w, while the fully connected fMRI network converges to $Q_w = 0$. In the limit of $r \to \infty$, the networks in which all edges have unique weights (i.e., a continuous weight distribution, which occurs in the empirical network as well as the ER network) converge to $Q_w = 0$, while the FH network, where by construction there exists multiple edges with the maximum edge weight, (i.e., a discrete weight distribution) converge to a non-zero value of $Q_w(r)$. Networks with continuous rather than discrete weight distributions display a peak in $Q_w(r)$, but the r value at which this peak occurs (r_{peak}, marked by a dot on each curve in Fig. 3) differs for each network. The conventional measurement of weighted modularity Q_w is associated with the value for $r=1$ (i.e. the original adjacency matrix), marked by the vertical dashed line in Fig. 3. In comparing curves it is clear that the conventional measurement (a single point) fails to extract the more complete structure obtained by computing the MRF using soft thresholding.

Summary. The results presented in Fig. 2 and Fig. 3 provide two types of diagnostic curves that illustrate features of the underlying weight distribution and network geometry. The curves themselves and the value of r_{peak} in Fig. 3 could be used to uncover differences in multiresolution network structure, for example in healthy versus diseased human brains. However, because the value of Q_w is dominated by a few edges with the largest weights, the identification of community structure in weak
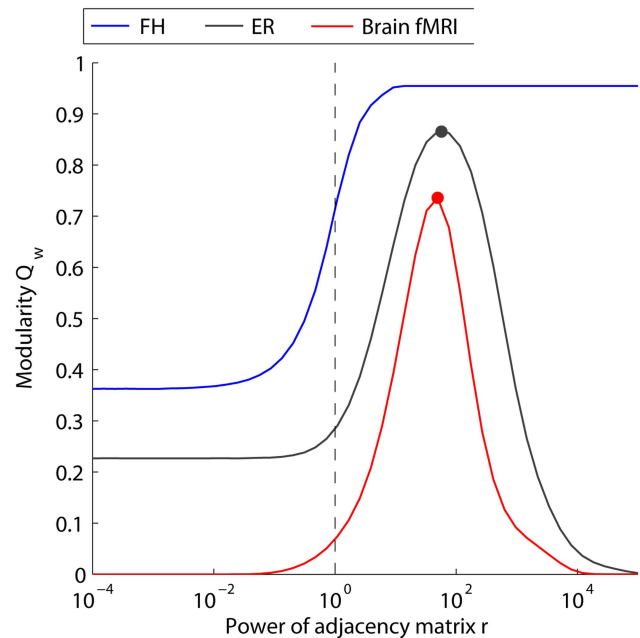
or medium-strength edges requires an entirely separate mathematical approach that probes the pattern of edges as a function of their weight, such as is provided by windowed thresholding (see next section).

Determining Network Differences in Multiresolution Structure

In this section, we examine Problem 2: Determining Network Differences in Multiresolution Structure. Determining differences in multiresolution network structure requires a set of techniques that quantify and summarize this structure in mesoscopic response functions of network diagnostics. Windowed thresholding is a unique candidate technique in that it resolves network structure associated with sets of edges with different weights. The technique decomposes a weighted adjacency matrix into a family of graphs. Each graph in this family shares a window size corresponding to the percentage of edges in the original network retained in the graph. A family of graphs is therefore characterized by a control parameter corresponding to the mean weight g of edges within the window. As we illustrate below in the context of network modularity and bipartivity, this control parameter can be optimized to uncover differences in multiresolution structure of networks.

Modularity. The modularity MRF $Q_b(g)$ as a function of weight g distinguishes between different networks in both its shape and its limiting behavior (see Figure 4A–C). The fractal hierarchical model (FH) yields a stepwise increase in modularity, where each step corresponds to one hierarchical level. The small world model (SW) illustrates two different regimes corresponding to (i) the random structure of the weakest 60% of the connections and
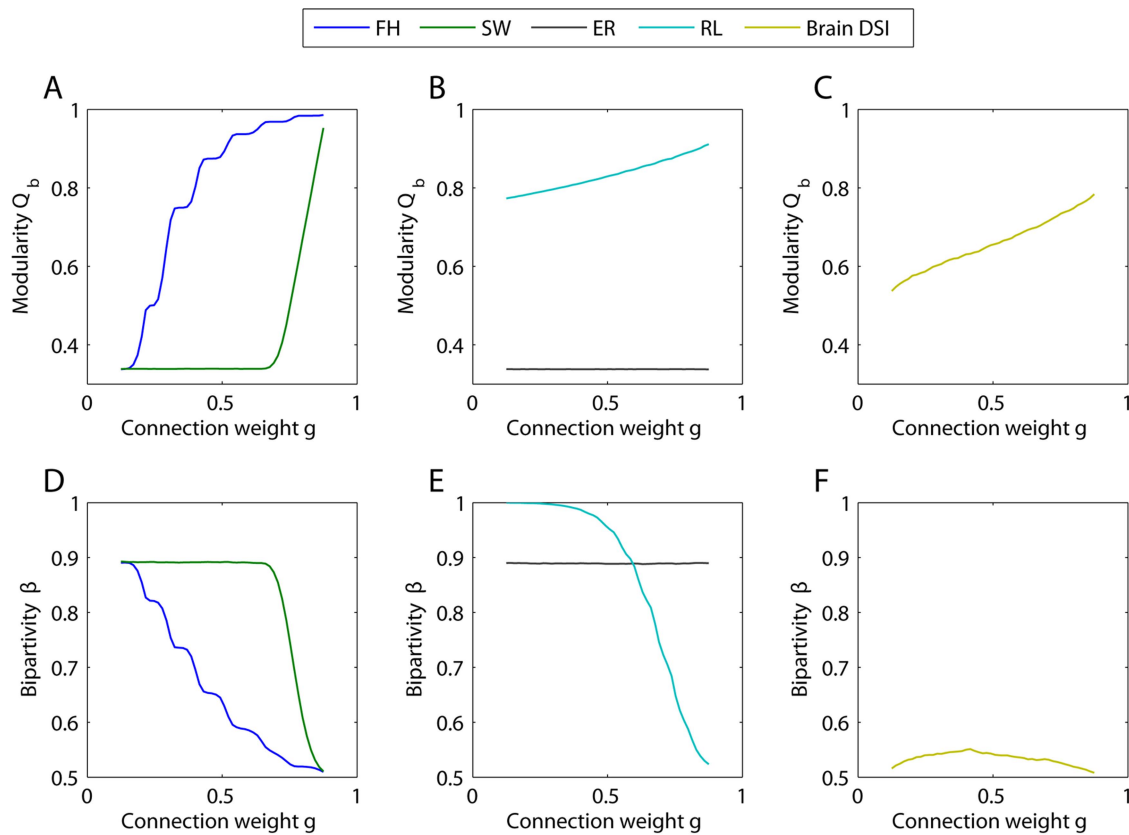
Figure 4. Mesoscale diagnostics as a function of connection weight. (A–C) Modularity as a function of the average connection weight g (see Methods Section) for fractal hierarchical, small world (B), Erdös-Rényi random, regular lattice (C) and structural brain network (D). The results shown here are averaged over 20 realizations of the community detection algorithm and over 50 realizations of each model (6 subjects for the brain DSI data). The variance in the measurements is smaller than the line width. (D–F) Bipartivity as function of average connection weight of the fractal hierarchical, small world, Erös-Rényi random model networks and the DSI structural brain networks. We report the initial benchmark results for a window size of 25% but find that results from other window sizes are qualitatively similar (see the Supporting Information).
doi:10.1371/journal.pcbi.1003712.g004

(ii) the perfectly modular structure of the strongly connected elementary groups. The Erdös-Rényi network (ER) exhibits no weight dependence in modularity, since the underlying topology is constant across different weight values. The ring lattice exhibits an approximately linear increase in modularity, corresponding to the densely interconnected local neighborhoods of the chain. The structural brain network exhibits higher modularity than ER graphs over the entire weight range, with more community structure evident in graphs composed of strong weights.

Bipartivity. The bipartivity MRF $\beta(g)$ as a function of weight g also distinguishes between different networks in both its shape and its limiting behavior (see Fig. 4C–E). The bipartivity of the Erdös-Rényi network serves as a benchmark for a given choice of the window size, since the underlying uniform structure is perfectly homogeneous, and $\beta(g)$ therefore only depends on the connection density of the graph. The small world model (SW) again shows two different regimes corresponding to (i) the random structure of the weakest 60% of the connections and (ii) the perfectly modular (or anti-bipartite [48]) structure of the strongly connected elementary groups. The fractal hierarchical model shows a stepwise decrease in bipartivity, corresponding to the increasing strength of community structure at higher levels of the hierarchy. The regular chain lattice model shows greatest bipartivity for the weakest 50% of connections and lowest bipartivity for the strongest 50% of connections. Intuitively, this behavior stems from the fact that the weaker edges link nodes to neighbors at farther distances away, making a delineation into two sparsely intra-connected subgroups more fitting.

Summary: In all model networks, the bipartivity shows the opposite trend as that observed in the modularity (compare top and bottom rows of Figure 4), supporting the interpretation of bipartivity as a measurement of "anti-community" structure [48]. It is therefore of interest to note that the DSI brain data shows very low bipartivity (close to the minimum possible value of 0.5) over the entire weight range, consistent with its pronounced community structure over different weight-based resolutions.

Uncovering differential structure in edge strength & length. In this section, we examine Problem 3: Uncovering Differential Structure in Edge Strength & Length. Unlike the synthetic networks, human brain networks are physically embedded in the 3-dimensional volume of the cranium. Each node in the network is therefore associated with a set of spatial coordinates and each edge in the network is associated with a distance between these coordinates. MRFs for network diagnostics can be used to compare this physical embedding with the network's structure, and, as we show below, could offer particular utility in uncovering neurophysiologically relevant individual differences in network architecture.

To illustrate the utility of this approach, we extract MRFs using two different measures of connection weight g for structural DSI brain data (see Figure 5). In one case g is the density of fiber tracts between two nodes, and in the other case g is the length of the
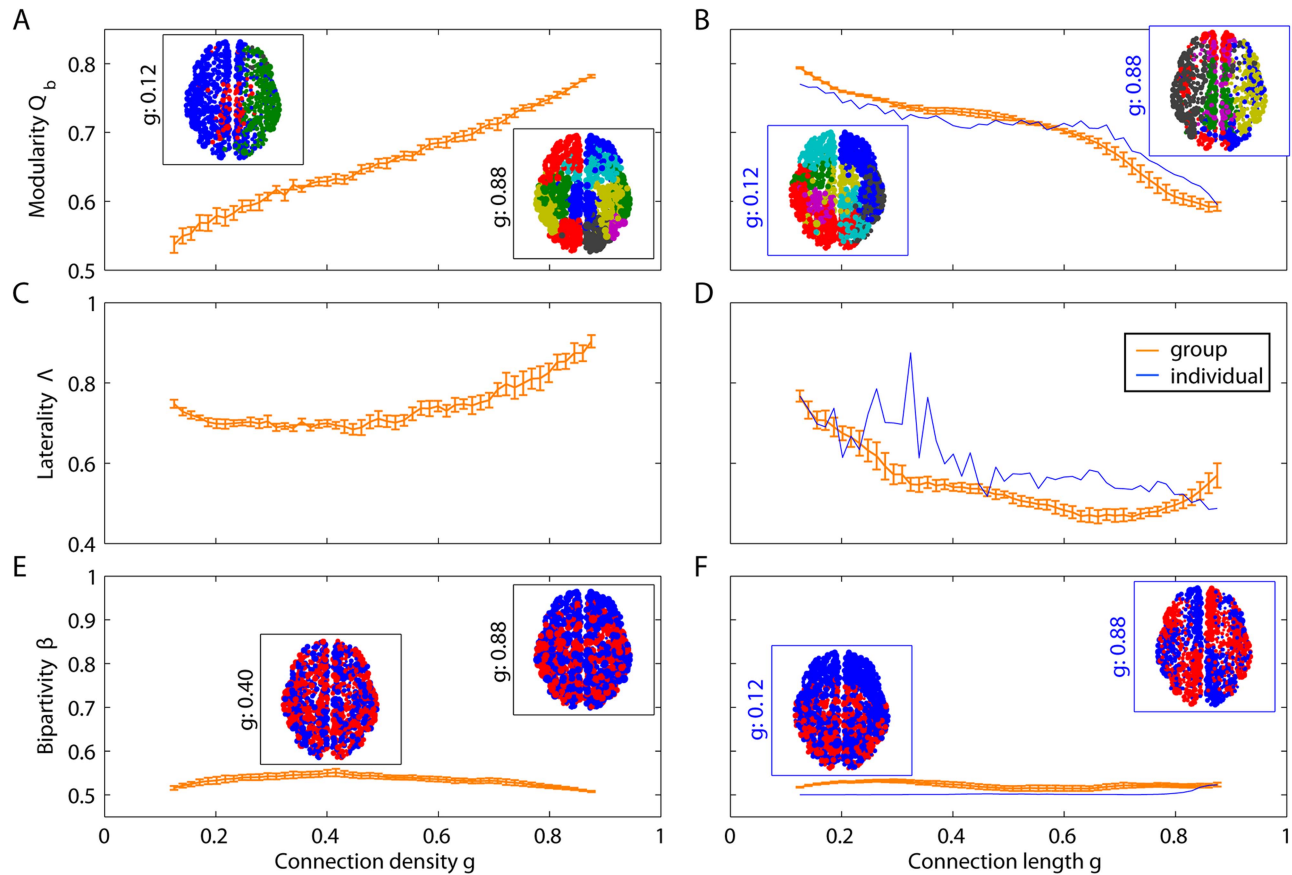
Figure 5. Effect of connection density and length on mesoscale diagnostics. *(A–B)* Modularity Q_b, *(C–D)* laterality Λ and *(E–F)* bipartivity β as a function of the fiber tract density density *(A,C,E)*, fiber tract arc length *(B,D,F, blue curve)* and Euclidean distance *(B,D,F, orange curve)*. Orange curves correspond to the mean diagnostic value over DSI networks; blue curves correspond to the diagnostic value estimated from a single individual. The orange curves in panels *B*, *D*, and *F* represent the Euclidean distance between the nodes; the blue curve represents the average arc length of the fiber tracts. The insets illustrate partitions of one representative data set (see the Methods Section), indicating that communities tend to span the two hemispheres thus leading to low values of bipartivity. All curves and insets were calculated with a window size of 25%.
doi:10.1371/journal.pcbi.1003712.g005

connections, measured by Euclidean distance or tract length. High density and short length edges tend to show more prominent community structure (higher $Q_b(g)$), with communities tending to be isolated in separate hemispheres (higher $\Lambda(g)$). Low density and long edges tend to show less prominent community structure (lower $Q_b(g)$), with communities tending to span the two hemispheres (lower Λ). Bipartivity peaks for long fiber tract arc lengths, corresponding to the separation of the left and right hemisphere which is even more evident in smaller window sizes (see Supplementary Information). These results suggest a relationship between spatial and topological structure that can be identified across all edge weights and lengths.

The shapes of the MRFs are consistent across individuals. The small amount of inter-individual variability in $Q_b(g)$ and $\beta(g)$ is observed in graphs composed of weak edges. Weak connections may be (i) most sensitive to noise in the experimental measurements, or (ii) most relevant to the biological differences between individuals [15]. Further investigation of individual differences associated with weak connections is needed to resolve this question.

Identifying Physical Correlates of Multiresolution Structure

In this section, we examine Problem 4: Identifying Physical Correlates of Multiresolution Structure. Windowed thresholding

enables us to separately probe the organization of edges according to specific properties that define their weights (e.g., weak versus strong, long versus short, etc.). This prevents strong edge weights from dominating the measurements. However, an important limitation of this method is that network diagnostics are restricted to a particular class of nodes within each window, and thus this method potentially misses important structure associated with the topology connecting different geometrical scales. Here we illustrate methods to combine these sources of information, and demonstrate that small communities in human anatomical brain networks tend to be geographically localized while large communities tend to be geographically distributed.

To probe community structure at different geometrical scales, we employ a complementary approach. By tuning the resolution parameter γ in the optimization of the modularity quality function (Equations 1 and 2), we can identify partitions of the network into both many small (high γ) and a few large (low γ) communities (see). Compared to our other control parameters, the resolution parameter tunes the output of a diagnostic (e.g. the number of communities), rather than acting directly in the edge weights themselves.

Varying γ allows us to probe several features of the network. First, we can uncover the fragmentation profile of a network, as illustrated in Fig. 6A. For example, in brain DSI networks, the
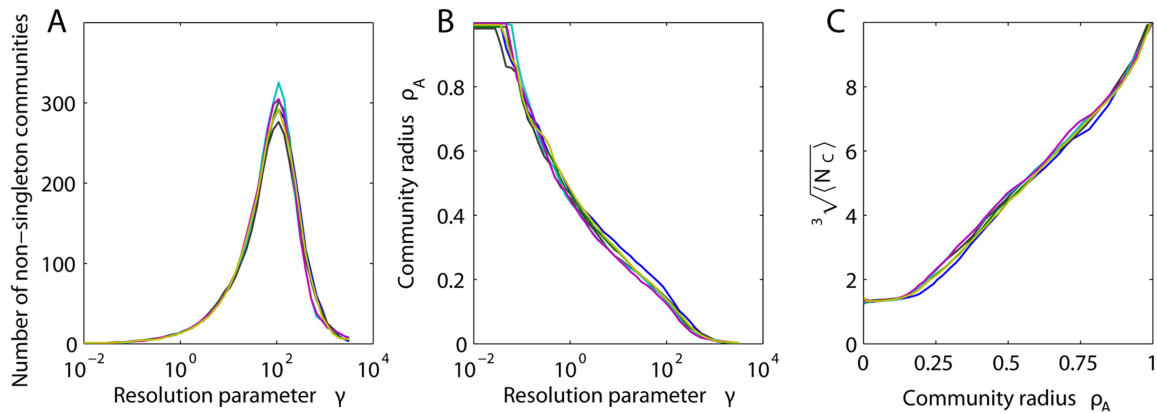
Figure 6. Effect of the resolution parameter on measured community structure. *(A)* Number of non-singleton communities and *(B)* mean community radius ρ_A as a function of the resolution parameter γ. *(C)* Mean number of nodes per (non-singleton) community $\langle N_c \rangle$ as a function of ρ_A. Results are presented for networks extracted from the DSI data of six individuals, illustrating consistency across subjects.
doi:10.1371/journal.pcbi.1003712.g006

number of non-singleton communities peaks at approximately $\gamma = 100$, after which the network fragments into isolated nodes. Second, we can probe the relationship between community structure and physical network embedding. We observe a polynomial relationship between community radius and the resolution parameter (see Fig. 6B) and by extension the number of nodes in the community (Fig. 6C), highlighting the interdependence of geometrical and spatial structure in the brain. Small communities tend to be geographically localized while large communities tend to be geographically distributed, suggestive of efficient embedding [54]. Modular networks that are not efficiently embedded into physical space would demonstrate no such relationship. The interaction between space and topology could enhance the organization of information transmission and computing: smaller information processing tasks could be completed by local circuits while larger tasks might make use of more extensive connectivity patterns.

Demonstrating Clinical Relevance

In this section, we examine Problem 5: Demonstrating Clinical Relevance. A primary goal of the analysis of human brain networks is to identify changes in network architecture that relate to neurodegenerative diseases or mental disorders. In this section, we investigate the potential applications of multi-resolution techniques to group comparisons by comparing the MRFs for functional brain networks extracted from healthy controls to those extracted from people with schizophrenia. We demonstrate surprisingly that group differences can be located in graphs composed of weak edges.

Functional brain network architecture at rest [15,55,56] and during task performance [8,57,58] is known to be altered in schizophrenia [9,59], supporting the hypothesis that schizophrenia stems from large-scale brain *dysconnectivity* [60,61,62]. Indeed, we observe that the weighted modularity Q_w (obtained at the default resolution of $\gamma = 1$) is significantly higher in people with schizophrenia than it is in healthy controls (nonparametric permutation test: $p \doteq 0.001$; see Fig. 7A).

MRFs can be used to probe these dysconnectivities in novel ways. By varying γ, we demonstrate that this group difference is evident over a range of resolutions, corresponding to partitions with both somewhat smaller and somewhat larger communities (nonparametric permutation test of group differences between these curves: $p < 0.001$; see Fig. 7B). The MRF also shows that the community

structure over very small and very large communities is not different between the two groups, indicating that signatures of dysconnectivity can be constrained to specific resolutions.

To determine whether the patterns of relatively weak or relatively strong edges are most relevant to disease-related alterations in mesoscale brain network architecture, we use the windowed thresholding technique (see Fig. 7C). In both groups, graphs composed of strong edges display higher modularity $Q_b(g)$ than graphs composed of weak edges. However, group differences are predominantly located in graphs composed of either the strongest (high modularity) or weakest (low modularity) edges. No group difference is evident in the bulk of graphs constructed from edges with medium weights, which display modularity values similar to those of the Erdös-Rényi model at the same connection density. The surprising utility of weak connections in uncovering dysconnectivity signatures has been noted previously in the context of schizophrenia [15] and could potentially be of use in the study of other neuropsychiatric disorders and brain injury.

The organization of weak and strong edges is further elucidated by the MRFs for bipartivity $\beta(g)$ as a function of the connection weight g (see Fig. 7D). In both groups, bipartivity values are smallest for edges with large weights. This finding is consistent with those presented in Fig. 7C, indicating that strong edges tend to be well localized within functional communities. In general, we observe significantly larger values of bipartivity in people with schizophrenia than in controls (nonparametric permutation test: $p = 0.004$). This difference is spread approximately evenly across the entire range of connection weights, in contrast to the group differences in modularity which were localized to a specific resolution range.

Discussion

Functional and structural brain network organization displays complex features such as hierarchical modularity [20,23,54] and scaling relationships in both topological [28,63,64] and physical space [54]. However, the identification of these structures has largely depended on a binarization of inherently weighted networks. In this paper, we explore several complementary analytical techniques — including soft thresholding, windowed thresholding, and modularity resolution — to identify structure at varying scales in weighted brain graphs. We find that brain network structure is characterized by modularity and bipartivity mesoscopic response functions that are shaped unlike those of
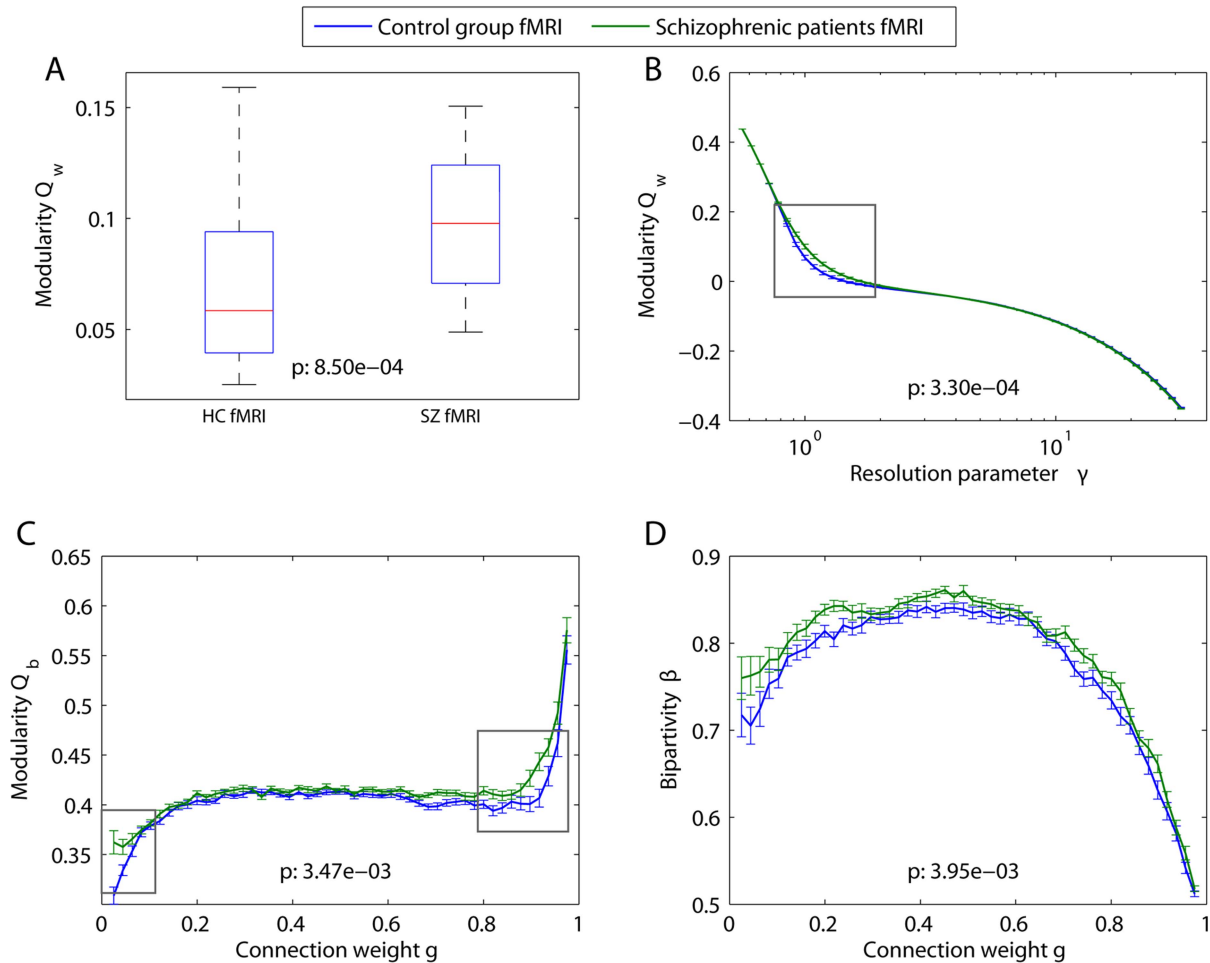
Figure 7. Multiresolution mesoscale structure in functional networks. Functional brain networks were extracted from resting state fMRI data acquired from 29 people with schizophrenia and 29 healthy controls [15] (see Methods Section). *(A)* Weighted modularity for healthy controls (left) and people with schizophrenia (right). Box plots indicate range and 25% (75%) quartiles over the individuals in each group. The structural resolution parameter is $\gamma = 1$. *(B)* MRFs for the weighted modularity as a function of the resolution parameter γ. *(C)* MRFs for binary modularity as a function of connection weight. *(D)* MRFs for bipartivity as a function of connection weight. In panels *(C)* and *(D)*, diagnostic values were estimated using a window size of 5%. In all panels, *p*-values for group differences in summary statistics (panel *(A)*) and MRFs (panels *(B–D)*) were calculated using a non-parametric permutation test [15]; resolutions displaying the strongest group differences are highlighted by gray boxes. In panels *(B–D)*, error bars show the standard deviation of the mean for healthy controls (blue) and people with schizophrenia (green).
doi:10.1371/journal.pcbi.1003712.g007

several synthetic network models. Moreover, the organization of these networks changes appreciably over topological, geometric, and spatial resolutions. Together, our results have important implications for understanding multiresolutions structure in functional and structural connectomes.

Multi-Resolution Topological Structure

Mesoscale structures—including modularity and bipartivity—display organization that is dependent on the weight of connections included in the network. The strongest connections in high resolution structural brain networks display stronger community structure, more lateralization of communities to the two hemispheres, and less bipartivity than the set of weakest connections. However, even the weakest connections display a modularity that is greater than expected in a random graph, suggesting the presence of nontrivial structure that might provide important insights into brain organization and function. These results are interesting in light of the fact that such connections have previously been thought to be driven purely by noise and are often

removed from the network for statistical reasons [65]. Our results that weak connections retain structure are consistent with recent evidence demonstrating the potential utility of studying the topology (binary) and geometry (weighted) of weak connections for diagnostic purposes [15].

Non-random structure in weak connections could stem from multiple factors – some more biologically interesting than others. First, experimental noise that is preferentially located in particular brain regions (e.g., fronto-temporal susceptibility artifacts) could lead to non-homogeneous network structure. Second, weak connections could be driven by different neurophysiological mechanisms than those driving strong connections (e.g., phase-lagged interactions would be measured as weak connections in correlation-based functional networks). In this case, the meso-scopic response functions would map out a transition between one mechanism for weak connections and another for strong connections. This latter possibility is potentially interesting from a clinical perspective because it could help to disambiguate the role of multiple mechanisms that could drive the altered connectivity

patterns evident in many disease states [8,66,67]. In this work, we have simply noted the presence of non-random structure in weak connections but we cannot disambiguate the role of these factors.

Multi-Resolution Spatial Structure

In addition to weight dependence, mesoscale structures also display organization that is dependent on the length of connections included in the network. Networks composed of relatively long connections show weaker community structure than networks composed of relatively short connections. This distributed nature of long connections is consistent with their hypothetical role in connecting disparate functional modules [68]. Furthermore, our results show that communities composed of long connections are more likely to span both hemispheres and display high bipartivity while those composed of shorter connections tend to be more lateralized and display weaker bipartivity, suggesting their role in both inter-hemispheric and inter-lobe communication.

To complement these analyses, we investigated the relationship between community structure and connection distance by employing the structural resolution parameter in the optimization of the modularity quality function. Our results demonstrate that modules composed of few nodes (i.e., community structure at fine-scale structural resolutions) have small spatial radii while those composed of more nodes (i.e., larger-scale structural resolutions) have larger spatial radii. Importantly, this mapping between structural and spatial resolutions would not be expected from a network randomly embedded into physical space [54]. Furthermore this relationship between structural resolution and spatial dimension of modules suggests a non-random but rather hierarchical organization within modules, since we find the sub-modules of each module to be have a smaller radius than the super-module. This would not be expected if the sub-structure of a module was randomly organized.

These results highlight the relationship between the geometry of a network (based on edge weights) and the physical embedding of that network into 3-dimensional space, a relationship which is of interest in a wide variety of complex systems [69]. Such a relationship is consistent with a large body of prior work demonstrating that brain networks extracted from a range of species tend to have near-minimal wiring [5,20,55,70,71,72], implicating a density of connections in local geographic neighborhoods and a sparsity of connections bridging those neighborhoods. In contrast to these previous studies that link physical distance to global (path-length and efficiency) and local (clustering coefficient and local efficiency) network diagnostics, our work uncovers the complementary influence of physical space on meso-scale structures (modularity and bipartivity).

The interaction between space and topology in brain systems could be driven by energetic and metabolic constraints on network development [3,20,54,73]. Such constraints might also play a role in the fine-grained spatial geometry of white matter fiber tracts, which cross one another at 90 degree angles [74], thereby potentially minimizing electromagnetic interference. Moreover, such constraints likely have important implications for system function, where short connections are potentially easier to maintain and use than long connections [75]. If such a functional consequence of physical constraints existed, it might partially explain the functional deficits observed in disease states associated with large-scale disconnectivity [59,64,75,76]. However, converse evidence from normal human development indicates that some distributed processing based on long distance connections is necessary for healthy cognitive function [77]. Future work is necessary to better understand the role of physical constraints on brain development and organization.

Brain Symmetries

While community structure in functional and structural brain networks has been examined in a number of studies [22,23,54,78], other types of mesoscale properties have been less studied. Here we employ two diagnostics – bipartivity and community laterality – that could capture signatures of one of the unusual properties of the brain compared to other complex systems: the physical symmetry between the two hemispheres. Our data suggest that such symmetry is observable in the organization of brain networks. The lateralization of communities is greatest for strong, local connections and smallest for weak, long-range connections, consistent with the preference for small modules to contain nodes in a local geographic neighborhood. Conversely, the bipartivity is greatest for mid-strength and long-range connections respectively and the two parts of the bipartite structure appear to map out both anterior-posterior and left-right axes of brain development. The putative functional role of these network symmetries is at least preliminarily supported by our finding that bipartivity of resting state functional brain networks in people with schizophrenia is significantly higher than that in healthy controls. Such whole-brain network signatures could derive from local asymmetries in white matter microstructure [79] and decreased interhemispheric white matter connectivity previously observed in schizophrenia [80].

Combining Multiresolution Techniques

In this paper, we have described several complementary techniques for uncovering multi-resolution structure in weighted networks. Each method has advantages and disadvantages and enables one to capture different features present in the network data. Here, for example, we have illustrated these techniques in probing the geometry (weak versus strong edges), embedding (short versus long edges), and structural resolution (small versus large communities) of network architecture. However, in some cases one might wish to probe multiple features of the network architecture simultaneously.

In Figure 8, we illustrate the combined use of the structural resolution parameter and windowed thresholding to elucidate the fragmentation profiles of empirical and synthetic network models. In the fractal hierarchical network, we observe that the banding of the number of communities as a function of the mean connection weight g is evident for small but not large values of the structural resolution parameter γ, indicating that the structural organization of the network can be hidden if one studies communities of small size. The remainder of the models and the empirical network data display a relatively constant number of communities over a broad range of mean connection weights for a given value of the structural resolution parameter γ. This consistency suggests, not surprisingly, that the number of communities is driven more by γ than by the underlying network topology, which for each of these networks (with the exception of the Erdös-Rényi model) varies over different mean connection weights. The band structure in the ER model is similar to the band structure in the SW model for weak edges (g less than approximately 0.70) because both sets of edges are randomly distributed: for the ER model, all connections are randomly distributed, and for the SW model, long-range connections (which are the weak edges in our weighting scheme) are randomly distributed. Therefore, both networks display the same geometry for weak edge weights but differ in the geometry of their strong edge weights. Unlike both the SW and ER models, the brain DSI network shows a decreasing number of communities as for stronger edge weights over a range of the resolution parameter. More similar to the fractal hierarchical network, this finding suggests that the human brain network displays hierarchical structure, with a few strong and large communities become
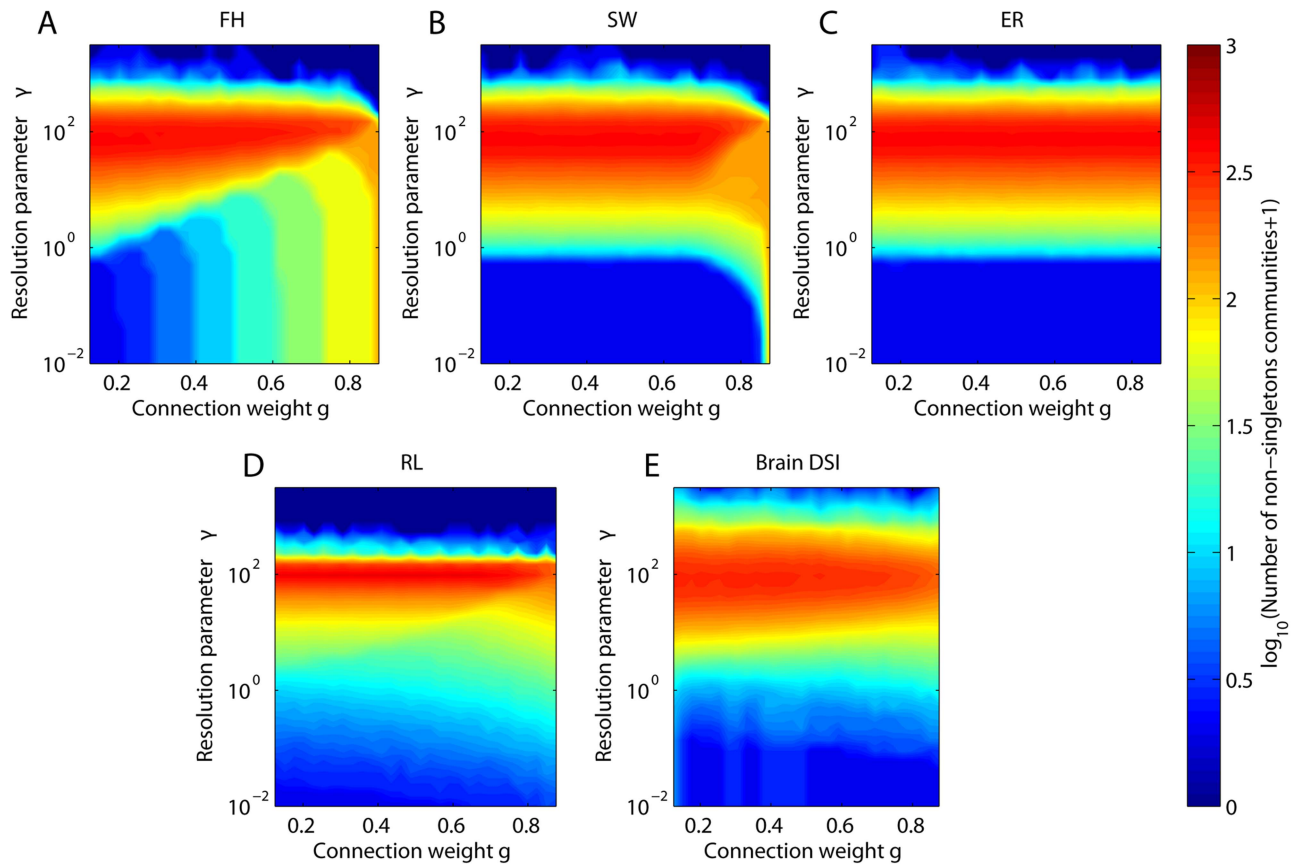
Figure 8. Simultaneously probing structural resolution and network geometry. Color plots of the number of non-singleton communities as function of both average connection weight g and resolution parameter γ for the *(A)* fractal hierarchical, *(B)* small world, *(C)* Erdös-Rényi, and *(D)* ring lattice, and for *(E)* one representative DSI anatomical network. The window size is 25%. For results of the total number of communities (singletons and non-singletons), see the Supporting Information.
doi:10.1371/journal.pcbi.1003712.g008

composed of many more weaker communities [54]. All networks completely fragment (zero non-singleton communities at high values of the structural resolution parameter) at similar but not identical values of γ, making comparisons across topologies for fixed γ difficult. We plan to investigate the combined use of these multi-resolution methods in more detail in future work.

Methodological Considerations

Models of brain structure. In this work we compared observed multi-resolution organization in brain networks to the organization expected in 4 synthetic networks. While many

synthetic network models exist for such a comparison, we chose two benchmark networks with local (ring lattice) and global (Erdös-Rényi) properties and two networks with mesoscale structures including community structure and hierarchical community structure. Our results show that none of these models displays similar modularity or bipartivity MRFs to those of the brain. An important area of investigation for future work is the generation of alternative synthetic network models that conserve additional network properties of brain systems or employ more biologically realistic growth mechanisms (see for example [28]). Moreover, we assigned the edge weights in these models in the simplest possible manner and these
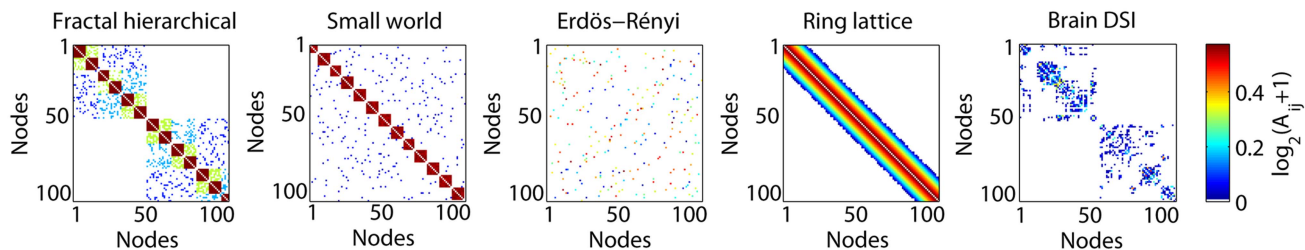

Figure 9. Weighted connection matrices for the synthetic benchmark networks and an empirical brain DSI network (N = 1000 nodes). Because network topologies can be difficult to decipher in large networks, here we illustrate the connections between only 100 of the total 1000 nodes. In each network, the topology changes as a function of edge weight (i.e., color) in the adjacency matrix. The windowed thresholding technique isolates topological characteristics in the subnetworks of nodes of similar weight. We report the initial benchmark results for a window size of 25% but find that results from other window sizes are qualitatively similar (see the Supporting Information).
doi:10.1371/journal.pcbi.1003712.g009

models therefore produce weight-dependent changes in topology by construction. Alternative weighting schemes could provide more sophisticated generative models of network geometries that more closely mimic brain structure.

Distance bias in anatomical networks. The diffusion spectrum imaging network contains an inherent distance bias [17], meaning that long distance connections have a lower probability of being included in the network than short distance connections. While Hagmann and colleagues did use a distance bias correction in the preprocessing of these networks, the most complete correction method remains a matter of ongoing debate [17]. It is possible that some distance bias remains in the current DSI data sets that might artifactually inflate the observed relationship between space and topology. Indeed, an important area of future work remains to understand the effect of local wiring probabilities (both real and artifactual) on observed network organization [81].

Conclusions

Our work demonstrates several benefits to the employment of multiresolution network analysis techniques. Such techniques enable statistically meaningful assessments of the organization of weighted spatial networks as a function of edge density, length, and location in Euclidean space. The ability to resolve mesoscale properties – like modularity and bipartivity – over spatial and geometric scales facilitates a deeper understanding of network organization than is possible in the examination of any single resolution alone. Moreover, it enables more focused mechanistic hypotheses for altered connectivity profiles in clinical states where network organization might be perturbed in one resolution (weak or local connections) more than in another (strong or long connections).

Supporting Information

Figure S1 Optimization and realization variance. The optimization variance versus the realization variance in the *(A)* binary modularity and *(B)* number of communities for the ensembles of fractal hierarchical (blue), modular small-world (green), Erdös-Rényi (gray), ring lattice (cyan), and DSI brain (gold) networks. The dashed gray line indicates the the line of equivalence between the optimization and randomization variance.
(PDF)

Figure S2 Effect of multiresolution network geometry on community structure. *(A)* Weighted adjacency matrices depicted for 10% of nodes in the synthetic network models and structural brain networks extracted from DSI data. *(B-D)* Modularity Q_b as a function of the average connection weight g of the edges retained in the graph for the *(B)* fractal hierarchical, small world, *(C)*, Erdös-Rényi, regular lattice, and *(D)* structural brain network. Window size is 15%. Values of Q_b are averaged over 20 optimizations of the binary modularity quality function for each of 50 realizations of a synthetic network model or 6 subjects for the brain DSI network. The standard error of the mean is smaller than the line width.
(PDF)

Figure S3 Effect of multiresolution network geometry on bipartite structure. *(A)* Bipartivity as function of average connection weight g of the edges retained in the graph for the *(B)* fractal hierarchical, small world, *(C)*, Erdös-Rényi, regular lattice, and *(D)* structural brain network. Window size is 15%. Values of β are averaged over 50 realizations of a synthetic network model or 6 subjects for the brain DSI network. The standard error of the mean is smaller than the line width.
(PDF)

Figure S4 Role of singletons in community number and modularity. *(A)* Number of communities as a function of average connection weight g. *(B)* Number of singletons versus number of communities. Data points correspond to each graph in the family which captures network organization at different mean connection weights. *(C)* Number of non-singleton communities as a function of average connection weight g. *(D)* Binary modularity as a function of the number of singletons. The gray line shows the modularity of an Erdös-Rényi random network, when successively disconnecting nodes from the network and randomly adding the same number of connections in the rest of the network. Data points correspond to each graph in the brain DSI family which captures network organization at differen mean connection weights. Color indicates mean connection weight g. Window size is 15%. In panels *(A)* and *(C)*, error bars indicate the standard deviation of the mean; for the model networks this error is smaller than the line width.
(PDF)

Figure S5 Simultaneously probing structural resolution and network geometry. Colorplots of the total number of communities (singletons and non-singletons) as function of both average connection weight g and resolution parameter γ for the *(A)* fractal hierarchical, *(B)* small world, *(C)* Erdös-Rényi, and *(D)* regular lattice models and for *(E)* one representative DSI anatomical network. The window size is 25%.
(PDF)

Table S1 Description of network ensembles. The number of networks (size) in the ensemble, number of nodes, number of edges K given in units of $[10^3]$ edges for the two types of ensembles studied. Network Type I contains the brain DSI, Erdös-Rényi, Regular Lattice, Fractal Hierarchical, and Small World networks with $N = 1000$ nodes. Network Type II contains the brain fMRI, Erdös-Rényi, Regular Lattice, Fractal Hierarchical, and Small World networks with $N = 90$ nodes.
(PDF)

Text S1 Supplementary document including supplementary results on (i) Optimization and Realization Variance, (ii) Effects of Window Size, and (iii) Relationship Between the Number of Communities and Singletons.
(PDF)

Author Contributions

Conceived and designed the experiments: DSB JMC. Performed the experiments: CL. Analyzed the data: CL. Contributed reagents/materials/analysis tools: KOL DSB. Wrote the paper: CL DSB JMC.

References

1. Bassett DS, Meyer-Lindenberg A, Achard S, Duke T, Bullmore E (2006) Adaptive reconfiguration of fractal small-world human brain functional networks. Proc Natl Acad Sci USA 103: 19518–19523.
2. Bassett DS, Bullmore E (2006) Small-world brain networks. The Neuroscientist 12: 512–523.
3. Bullmore E, Sporns O (2009) Complex brain networks: graph theoretical analysis of structural and functional systems. Nat Rev Neurosci 10: 186–98.
4. Bullmore ET, Bassett DS (2011) Brain graphs: graphical models of the human brain connectome. Ann Rev Clin Psych 7: 113–140.
5. Kaiser M (2011) A tutorial in connectome analysis: topological and spatial features of brain networks. Neuroimage 57: 892–907.
6. Sporns O (2011) The human connectome: a complex network. Ann N Y Acad Sci 1224.
7. Stam CJ, van Straaten EC (2012) The organization of physiological brain networks. Clin Neurophysiol 123: 1067–87.

8. Bassett DS, Bullmore ET (2009) Human brain networks in health and disease. Curr Opin Neurol 22: 340–7.

9. Fornito A, Zalesky A, Pantelis C, Bullmore ET (2012) Schizophrenia, neuroimaging and connectomics. Neuroimage 62: 2296–2314.

10. Fornito A, Bullmore ET (2012) Connectomic intermediate phenotypes for psychiatric disorders. Front Psychiatry 3: 32.

11. He Y, Chen Z, Gong G, Evans A (2009) Neuronal networks in Alzheimer's disease. Neuroscientist 15: 333–350.

12. He Y, Evans A (2010) Graph theoretical modeling of brain connectivity. Curr Opin Neurol 23: 341–350.

13. van Wijk BCM, Stam CJ, Da_ertshofer A (2010) Comparing brain networks of different size and connectivity density using graph theory. PLoS ONE 5: e13701.

14. Ginestet CE, Nichols TE, Bullmore ET, Simmons A (2011) Brain network analysis: Separating cost from topology using cost-integration. PLoS ONE 6: e21570.

15. Bassett DS, Nelson BG, Mueller BA, Camchong J, Lim KO (2011) Altered resting state complexity in schizophrenia. NeuroImage, Schizophrenia 59: 2196–2207.

16. Fornito A, Zalesky A, Breakspear M (2013) Graph analysis of the human connectome: Promise, progress, and pitfalls. Neuroimage 80: 426–444.

17. Hagmann P, Cammoun L, Gigandet X, Meuli R, Honey CJ, et al. (2008) Mapping the structural core of human cerebral cortex. PLOS Biology 6: e159.

18. Porter MA, Onnela JP, Mucha PJ (2009) Communities in networks. Not Amer Math Soc 56: 1082–1097, 1164–1166.

19. Fortunato S (2010) Community detection in graphs. Phys Rep 486: 75–174.

20. Bassett DS, Brown JA, Deshpande V, Carlson JM, Grafton ST (2011) Conserved and variable architecture of human white matter connectivity. NeuroImage 54: 1262–1279.

21. Gallos LK, Sigman M, Makse HA (2012) The conundrum of functional brain networks: small-world efficiency or fractal modularity. Front Physiol 3: 123.

22. Meunier D, Lambiotte R, Fornito A, Ersche KD, Bullmore ET (2009) Hierarchical modularity in human brain functional networks. Front Neuroinform 3: 37.

23. Meunier D, Lambiotte R, Bullmore ET (2010) Modular and hierarchically modular organization of brain networks. Front Neurosci 4: 200.

24. Zhou C, Zemanová L, Zamora G, Hilgetag CC, Kurths J (2006) Hierarchical organization unveiled by functional connectivity in complex brain networks. Phys Rev Lett 97: 238103.

25. Wang SJ, Hilgetag CC, Zhou C (2011) Sustained activity in hierarchical modular neural networks: self-organized criticality and oscillations. Front Comput Neurosci 5: 30.

26. Kaiser M, Hilgetag CC (2010) Optimal hierarchical modular topologies for producing limited sustained activation of neural networks. Front Neuroinform 4: 8.

27. Rubinov M, Sporns O, Thivierge JP, Breakspear M (2011) Neurobiologically realistic determinants of self-organized criticality in networks of spiking neurons. PLoS Comput Biol 7: e1002038.

28. Klimm F, Bassett DS, Carlson JM, Mucha PJ (2014) Resolving structural variability in network models and the brain. PLoS Comp Biol 10: e1003491.

29. Doron KW, Bassett DS, Gazzaniga MS (2012) Dynamic network structure of interhemispheric coordination. Proc Natl Acad Sci U S A 109: 18661–18668.

30. Tzourio-Mazoyer N, Landeau B, Papathanassiou D, Crivello F, Etard O, et al. (2002) Automated anatomical labeling of activations in SPM using a macroscopic anatomical parcellation of the MNI MRI single-subject brain. Neuroimage 15: 273–289.

31. Camchong J, MacDonald III AW, Bell C, Mueller BA, Lim KO (2009) Altered functional and anatomical connectivity in schizophrenia. Schizophrenia Bulletin 37: 640–650.

32. Rubinov M, Sporns O (2010) Complex network measures of brain connectivity: Uses and interpretations. NeuroImage 52: 1059–69.

33. Sporns O (2006) Small-world connectivity, motif composition, and complexity of fractal neuronal connections. BioSystems 85: 55–64.

34. Onnela JP, Fenn DJ, Reid S, Porter MA, Mucha PJ, et al. (2012) Taxonomies of networks from community structure. Phys Rev E 86.

35. Travers J, Milgram S (1969) An experimental study of the small world problem. Sociometry 32: 425–443.

36. Watts DJ, Strogatz SH (1998) Collective dynamics of 'small-world' networks. Nature 393: 440–442.

37. Ravasz E, Barabási AL (2003) Hierarchical organization in complex networks. Phys Rev E 67: 026112.

38. Newman MEJ (2010) Networks - An Introduction. Oxford University Press, 1st edition.

39. Newman ME (2004) Fast algorithm for detecting community structure in networks. Phys Rev E 69: 066133.

40. Newman MEJ, Girvan M (2004) Finding and evaluating community structure in networks. Phys Rev E 69: 026113.

41. Newman MEJ (2006) Modularity and community structure in networks. Proceedings of the National Academy of Sciences 103: 8577–8582.

42. Blondel VD, Guillaume JL, Lambiotte R, Lefebvre E (2008) Fast unfolding of community hierarchies in large networks. J Stat Mech: P10008.

43. Jutla IS, Lucas GSJ, Mucha PJ (2011–2012) A generalized louvain method for community detection implemented in matlab. http://netwikiamathuncedu/GenLouvain/GenLouvain.

44. Traag VA, Bruggeman J (2009) Community detection in networks with positive and negative links. Phys Rev E 80: 036115.

45. Arenas A, Fernández A, Gómez S (2008) Analysis of the structure of complex networks at different resolution levels. New Journal of Physics 10: 053039.

46. Good BH, de Montjoye YA, Clauset A (2010) Performance of modularity maximization in practical contexts. Phys Rev E 81: 046106.

47. Estrada E, Rodríguez-Velázquez JA (2005) Spectral measures of bipartivity in complex networks. Phys Rev E 72: 046105.

48. Newman MEJ (2006) Finding community structure in networks using the eigenvectors of matrices. Phys Rev E 74: 036104.

49. Schwarz AJ, McGonigle J (2011) Negative edges and soft thresholding in complex network analysis of resting state functional connectivity data. NeuroImage 55: 1132–1146.

50. Zhang B, Horvath S (2005) A general framework for weighted gene co-expression network analysis. Statistical Applications in Genetics and Molecular Biology 4: 17.

51. Fortunato S, Barthélemy M (2006) Resolution limit in community detection. PNAS 104: 36–41.

52. Reichardt J, Bornholdt S (2006) Statistical mechanics of community detection. Physical Review 74: 016110.

53. Reichardt J, Bornholdt S (2007) Partitioning and modularity of graphs with arbitrary degree distribution. Phys Rev E 76: 015102.

54. Bassett DS, Greenfield DL, Meyer-Lindenberg A, Weinberger DR, Moore S, et al. (2010) Efficient physical embedding of topologically complex information processing networks in brains and computer circuits. PLoS Comput Biol 6: e1000748.

55. Lynall ME, Bassett DS, Kerwin R, McKenna P, Muller U, et al. (2010) Functional connectivity and brain networks in schizophrenia. J Neurosci 30: 9477–9487.

56. Rubinov M, Knock SA, Stam CJ, Micheloyannis S, Harris AW, et al. (2009) Small-world properties of nonlinear brain activity in schizophrenia. Hum Brain Mapp 30: 403–416.

57. Siebenhühner F, Weiss SA, Coppola R, Weinberger DR, Bassett DS (2012) Intra- and inter-frequency brain network structure in health and schizophrenia. arXiv 1209.0729.

58. Pachou E, Vourkas M, Simos P, Smit D, Stam CJ, et al. (2008) Working memory in schizophrenia: an EEG study using power spectrum and coherence analysis to estimate cortical activation and network behavior. Brain Topogr 21: 128–137.

59. Bassett DS, Bullmore ET, Meyer-Lindenberg A, Apud JA, Weinberger DR, et al. (2009) Cognitive fitness of cost-effcient brain functional networks. 106: 11747–11752.

60. Stephan KE, Baldeweg T, Friston KJ (2006) Synaptic plasticity and dysconnection in schizophrenia. Biol Psychiatry 59: 929–939.

61. Weinberger DR, Berman KF, Suddath R, Torrey EF (1992) Evidence of dysfunction of a prefrontallimbic network in schizophrenia: A magnetic resonance imaging and regional cerebral blood ow study of discordant monozygotic twins. Am J Psychiatry 149: 890–897.

62. Volkow ND, Wolf AP, Brodie JD, Cancro R, Overall JE, et al. (1988) Brain interactions in chronic schizophrenics under resting and activation conditions. Schizophr Res 1: 47–53.

63. Bassett DS, Siebenhühner F (2012) Multiscale Network Organization in the Human Brain, Wiley. Multiscale Analysis and Nonlinear Dynamics: From Genes to the Brain. 328 p.

64. Bassett DS, Bullmore E, Verchinski BA, Mattay VS, Weinberger DR, et al. (2008) Hierarchical organization of human cortical networks in health and schizophrenia. J Neurosci 28: 9239–9248.

65. Achard S, Salvador R, Whitcher B, Suckling J, Bullmore E (2006) A resilient, low-frequency, small-world human brain functional network with highly connected association cortical hubs. J Neurosci 26: 63–72.

66. Mengotti P, D'Agostini S, Terlevic R, De Colle C, Biasizzo E, et al. (2011) Altered white matter integrity and development in children with autism: a combined voxel-based morphometry and diffusion imaging study. Brain Res Bull 84: 189–95.

67. Sugranyes G, Kyriakopoulos M, Dima D, O'Muircheartaigh J, Corrigall R, et al. (2012) Multimodal analyses identify linked functional and white matter abnormalities within the working memory network in schizophrenia. Schizophr Res 138: 136–42.

68. Sporns O (2010) Networks of the Brain. MIT Press. 424 p.

69. Barthelemy M (2011) Spatial networks. Physics Reports 499: 1–101.

70. Kaiser M, Hilgetag CC (2006) Nonoptimal component placement, but short processing paths, due to long-distance projections in neural systems. PLoS Comput Biol 2: e95.

71. Chen BL, Hall DH, Chklovskii DB (2006) Wiring optimization can relate neuronal structure and function. Proc Natl Acad Sci U S A 103: 4723–4728.

72. Raj A, Chen YH (2011) The wiring economy principle: connectivity determines anatomy in the human brain. PLoS One 6: e14832.

73. Bullmore E, Sporns O (2012) The economy of brain network organization. Nat Rev Neurosci 13: 336–49.

74. Wedeen VJ, Rosene DL, Wang R, Dai G, Mortazavi F, et al. (2012) The geometric structure of the brain fiber pathways. Science 335: 1628–1634.

75. Vértes PE, Alexander-Bloch AF, Gogtay N, Giedd JN, Rapoport JL, et al. (2012) Simple models of human brain functional networks. Proc Natl Acad Sci U S A 109: 5868–5673.

76. Alexander-Bloch AF, Gogtay N, Meunier D, Birn R, Clasen L, et al. (2010) Disrupted modularity and local connectivity of brain functional networks in childhood-onset schizophrenia. Front Syst Neurosci 4: 147.

77. Fair DA, Cohen AL, Power JD, Dosenbach NU, Church JA, et al. (2009) Functional brain networks develop from a \local to distributed" organization. PLoS Comput Biol 5: e1000381.

78. Chen ZJ, He Y, Rosa-Neto P, Germann J, Evans AC (2008) Revealing modular architecture of human brain structural networks by using cortical thickness from MRI. Cereb Cortex 18: 2374–2381.

79. Miyata J, Sasamoto A, Koelkebeck K, Hirao K, Ueda K, et al. (2012) Abnormal asymmetry of white matter integrity in schizophrenia revealed by voxelwise diffusion tensor imaging. Hum Brain Mapp 33: 1741–1749.

80. Knöchel C, Oertel-Knöchel V, Schönmeyer R, Rotarska-Jagiela A, van de Ven V, et al. (2012) Interhemispheric hypoconnectivity in schizophrenia: fiber integrity and volume differences of the corpus callosum in patients and unaffected relatives. Neuroimage 59: 926–934.

81. Henderson JA, Robinson PA (2011) Geometric effects on complex network structure in the cortex. Phys Rev Lett 107: 018102.